



HAL
open science

Gas production reveals the metabolism of immobilized *Chlorella vulgaris* during different trophic modes

Jing Zhang, Patrick Perré

► **To cite this version:**

Jing Zhang, Patrick Perré. Gas production reveals the metabolism of immobilized *Chlorella vulgaris* during different trophic modes. *Bioresource Technology*, 2020, 315, pp.123842. 10.1016/j.biortech.2020.123842 . hal-03141449

HAL Id: hal-03141449

<https://hal.science/hal-03141449>

Submitted on 22 Aug 2022

HAL is a multi-disciplinary open access archive for the deposit and dissemination of scientific research documents, whether they are published or not. The documents may come from teaching and research institutions in France or abroad, or from public or private research centers.

L'archive ouverte pluridisciplinaire **HAL**, est destinée au dépôt et à la diffusion de documents scientifiques de niveau recherche, publiés ou non, émanant des établissements d'enseignement et de recherche français ou étrangers, des laboratoires publics ou privés.



Distributed under a Creative Commons Attribution - NonCommercial 4.0 International License

Gas production reveals the metabolism of immobilized *Chlorella vulgaris* during different trophic modes

Jing Zhang, Patrick Perré*¹

Université Paris-Saclay, CentraleSupélec, Laboratoire de Génie des Procédés et Matériaux, SFR Condorcet FR CNRS 3417, Centre Européen de Biotechnologie et de Bioéconomie (CEBB), 3 rue des Rouges Terres 51110 Pomacle, France

Abstract

The metabolism of heterotrophic and mixotrophic cultivation modes of *Chlorella vulgaris*, a potential source of biofuel and CO₂ mitigation, was studied in immobilized cultures. The gas concentration (O₂ and CO₂) was measured thanks to an original device manufactured using 3D printing. The biomass was monitored by 3D imaging and image processing. Net O₂ and CO₂ sources were obtained by a balance equation considering a calibrated leakage and the dissolved gas. Combined experimental and theoretical gas yields (mass of gas per mass of biomass), the photosynthesis proportion of mixotrophic colony was determined. Its increase with light intensity is not linear. Therefore, the highest light intensity ($104\mu\text{mol} \cdot \text{m}^{-2} \cdot \text{s}^{-1}$) revealed the limit of photosynthesis potential in the growth of mixotrophic colony. In the presence of light, the colony adopts a cylindrical shape instead of a spherical cap. This study proposed mechanisms of synergy inside the colony for heterotrophic and mixotrophic modes.

Keywords

Immobilized culture, Respiration, Photosynthesis, Heterotrophic, Mixotrophic

¹ * Corresponding author. E-mail address: patrick.perre@centralesupelec.fr (P. Perré).

1. Introduction

The most recent IPCC report concluded that reduction of CO₂ emissions resulting from the conversion to renewable resources would not be sufficient: carbon sequestration is mandatory (IPCC, 2019). *Chlorella vulgaris* attracts substantial attention: firstly, it is a potential biofuel resource, demonstrating rapid growth and high lipid content as a non-food competitiveness resource that can live on wastewater (Gouveia, 2007; Amit and Ghosh, 2019; Amit et al., 2020); secondly, it is a phototroph which could capture CO₂. In particular, designs have been proposed for the production of microalgae as biofilms rather than in suspension (Bernard et al., 2018; Blanken et al., 2014), which requires a better understanding of immobilized culture.

Generally, *C. vulgaris* is recognized as having three modes of cultivation: photoautotrophy, heterotrophy, and mixotrophy. In photoautotrophic mode, microalgae utilize inorganic carbon as a carbon source and light as an energy source. It is the most common and energy-saving mode and presents fewer contamination problems (Mohan et al., 2019). Heterotrophic mode utilizes organic carbon as both an energy and carbon source. It offers several advantages such as biomass and lipid productivity (Rattanapoltee and Kaewkannetra, 2014), cheaper and simpler bioreactor design, easier scaling-up process, changeable biomass composition, and potential wastewater treatment (Hu et al., 2018; Perez-Garcia and Bashan, 2015). In mixotrophic mode, *C. vulgaris* utilizes inorganic carbon and organic carbon as carbon sources, together with light and organic carbon as energy sources. This trophic mode expands the exponential growth phase, reduces biomass loss during dark respiration and the need for organic nutrient supplements (Sa et al., 2014), reduces or stops the photo-inhibitory effect, provides the flexibility to switch the metabolism mode, and protects against photo-oxidative damage (Mohan et al., 2019). Additionally, the in situ O₂/CO₂ cycle in mixotrophic cultivation mode could reduce energy waste from the CO₂ capture process

and prevent the harmful influence on the environment taking place before being converted. Considering the efficiency of productivity, in the current work, we focused on the mixotrophic and heterotrophic cultivation modes.

Light intensity affects the photosynthesis of algae (Darvehei et al., 2018). Three zones might be sequentially distinguished when light intensity increases: light limitation, saturation, and inhibition. However, the role of light intensity in the mixotrophic culture mode is still poorly defined. Ogbonna et al. (2002) reported that the mixotrophic culture of *Euglena gracilis* was more sensitive to photoinhibition than photoautotrophic culture. In contrast, Chojnacka and Marquez-Rocha (2004) reviewed that no photoinhibition was observed in the mixotrophic cultivation, whereas it was observed in the photoautotrophic cultivation when the light intensity was above $270\mu\text{mol} \cdot \text{m}^{-2} \cdot \text{s}^{-1}$. This is one of the interests that brings us to the current study.

Understanding the metabolism in each cultivation mode would help to control and enhance the performance of cultures in both industrial and academic applications. The mixotrophic cultivation mode is worthy of study as it is complex and thus far poorly understood. The specific growth rate has been employed to study the relationship between these three cultivation modes and reported that the mixotrophic growth rate of microalga could be less than, equal to, or higher than the sum of the other two modes (Kong et al., 2011; Martínez and Orús, 1991; Ogbonna et al., 2002). The respiration and photosynthesis metabolisms may be concurrent and independent under mixotrophic mode, and the observed growth change might be caused by the local enzyme and substrate of each pathway variation. Ogbonna et al. (2002) reported that the specific growth rate of mixotrophic growth equals the sum of the photoautotrophic and heterotrophic growth when the light supply coefficient is low, while the mixotrophic is smaller than the sum of the other two when the light supply coefficient is high. Mirzaie et al. (2016) reported that heterotrophic growth dominated the initial growth days, then

autotrophy in the mixotrophic growth became dominant, while others have argued for the inverse order (Ayed et al., 2017; La et al., 2019).

Oxygen and carbon dioxide are both involved in photosynthesis and respiration, the two main bioenergetic processes of microalgae (Cournac et al., 2002). Oxygen is generated through photosynthesis, while it is consumed in metabolic reactions such as mitorespiration (mitochondrial consumption), photorespiration, chlororespiration, and the Mehler reaction (Lewitus and Kana, 1995). Data on the evolution of oxygen and carbon dioxide, dry weight growth, and population growth are essential to understand the metabolic characteristics of *C. vulgaris* in different trophic modes. In practice, in any photobioreactor design, the autoshading effect imposes non-uniform lighting (Shoener et al., 2019). Together with the liquid flow, this induces spatial and temporal variation in the population. In this sense, the balance between different modes and the time required to change the metabolism are of crucial importance (Han, 2001; Pozzobon and Perré, 2018).

Monitoring gas fluxes may be the best way to assess the averaged effect in space and time. Gas production, especially oxygen and carbon dioxide, is generally determined by comparing the difference between the inlet and outlet flux (Molina et al., 2001), which can be performed by external integrated sensors (La et al., 2019) or by respirometry methods (Tang et al., 2014). They are all used in suspensions, for which the gas solubility is estimated using Henry's law. Microelectrode sensors could measure the trace concentrations of oxygen but need to be inserted into the culture/biofilm (Rincon et al., 2017). **In our device, embedded gas sensors allowed us to monitor the gas concentration continuously and a transparent cover was employed to measure the biomass cumulation non-destructively through 3D imaging.**

In the present study, these devices and a structured-light microscope, the volume, equivalent radius, height, and morphology development of a colony were observed concomitant with the gas evolution. The colony productivity was assessed within different tropic modes and light intensities. The entire dataset, combining the variation of biomass and gas production/consumption, allowed for the metabolism of the colony to be inferred as a function of growth conditions.

2. Materials and Methods

2.1. Strain and media

Chlorella vulgaris SAG 211-12 (Culture Collection of Algae [SAG], University of Göttingen, Germany) was pre-cultured in B3N liquid medium (Clément-Larosière et al., 2014) at room temperature, 170rpm, under $50 \mu\text{mol} \cdot \text{m}^{-2} \cdot \text{s}^{-1}$ continuous LED illumination on the culture surface. Colonies were grown on MBM-GP solid medium (La et al., 2019). This medium contains $20\text{g} \cdot \text{L}^{-1}$ agar and organic carbon sources in the combined form of $20\text{g} \cdot \text{L}^{-1}$ peptone and $10\text{g} \cdot \text{L}^{-1}$ glucose (D(+)) glucose, $\geq 99\%$, anhydrous, ACROS Organics™, Czech Rep). Approximately 15mL medium were allowed to solidify in a 50mm diameter Petri dish, and a nitrocellulose membrane (0.2 μm pore, 47mm diameter, Sartorius Stedim Biotech GmbH, Germany) was placed on the surface of the medium to support colonies.

2.2. Experiment

2.2.1. Calibration of specific growth rate

MBM-GP liquid medium was used for the mixotrophic and heterotrophic *C. vulgaris* cultivation, and B3N medium for the photoautotrophic cultivation. The 7-day-old pre-culture was inoculated into media (50mL in 250mL Erlenmeyer flask) at a ratio of 1%v/v at an initial density of $1.2 \times 10^7 \text{ cell/mL}$. All cultures were placed in a 25°C incubator under continuous light (LED, 3.5W, 260lm, 35°, 4000K, 220–240V, 50Hz, 30mA, China) and magnetically stirred at a constant speed. The mixotrophic and

photoautotrophic culture was exposed to a continuous LED illumination with an intensity of $60 \pm 10 \mu\text{mol} \cdot \text{m}^{-2} \cdot \text{s}^{-1}$ reaching the surface of the flask, and the heterotrophic culture was covered with aluminum foil to avoid any illumination. Each culture treatment was performed in duplicate.

2.2.2. Oxygen and carbon dioxide monitoring equipment

To monitor O₂ and CO₂ concentration (noted as [O₂] and [CO₂]) during colony growth, in-house devices containing cavities for two gas sensors and one 50-mm Petri dish were designed (Fig. 1). The housing was printed using ABS (acrylonitrile butadiene styrene) material and coated with epoxy resin (Yachtcare, SOLOPLAST VOSSCHEMIE, France) to increase airtightness. The inlet and outlet of housing added to allow leakage calibration, were sealed with hot glue then coated with epoxy resin (ACROS Organics™, Czech Rep) during the experiment aimed at minimizing the housing leak.

The CO₂ sensor (ExplorIR®-M CO₂ Sensor, GSS, UK) has a range of 0–5%. This sensor works with a non-dispersive infrared (NDIR) gas sensing method: CO₂ is measured by monitoring the amount of infrared light being absorbed by CO₂ gas. The accuracy is $\pm(70\text{ppm} + 5\%$ of the reading). Sensors were calibrated by setting the indication at 0.04% after stabilization in fresh air without a lid.

The O₂ sensor (LuminOx Sealed O₂ Sensors, SST Sensing Ltd, UK) works within the range of 0–25%, combined with an internal sensor for total pressure and temperature. The O₂ sensor works on the luminescence quenching principle: the oxygen molecules quench the fluorescence intensity release from an organometallic fluorescent dye, and the ppO₂ is proportional to the fluorescence intensity and lifetime. No O₂ is consumed during the measurement. The measured quantity is the partial pressure of oxygen (ppO₂), which is converted to oxygen concentration (O₂%) using the total pressure measurement. The resolution of O₂ concentration is 0.01%, pressure, 1mbar, at a temperature of 0.1°C.

The accuracy is $\text{ppO}_2 < 2\%$ full scale, and $\pm 5\text{mbar}$. Sensors were calibrated after stabilization in fresh air without a lid. All readings were subsequently scaled by the ratio of $20.9/([\text{O}_2] \text{ read in fresh air})$.

2.2.3. Inoculation

To amplify the gas signal, ten identical colonies were inoculated onto a Petri dish for each experiment. The initial distance between neighboring colonies was greater than 9mm, which prevented physical contact through the entire experiment duration. Sampling procedures have been described previously (Zhang et al., 2020). Briefly, 10mL liquid 7-day-old pre-cultures were centrifuged for 5 minutes at 4°C at 8586 g (Centrifuge, 5804 R, Eppendorf, Germany) using a 15mL tube and then centrifuged for another 5 minutes at 4°C at 6800 g in a 1.5mL tube. Finally, a trace of cells, approximately 1.7×10^5 cells, was transferred from the pellet onto the membrane by a $2.5\mu\text{L}$ micro-tip cautiously. The initial cells number of the colony as an inoculum was determined using a Beckman Coulter counter (MultisizerTM 4 COULTER COUNTER[®], California, United States), as described previously (Zhang et al., 2020): transferring the colony to Milli-Q water (BioPak[®]), resuspending and mixing the suspension to a homogeneous one, determining the cell concentration by Coulter counter, and calculating the cells number as the product of cell concentration times the dilution folds. Note that the cell enumeration procedure is a destructive one, therefore, the initial cells number was denoted by an average value of eight extra colonies. Meanwhile, their volumes were measured by 3D imaging and compared to those inoculums used in the experiments, which improves the confidence of the stability of size of each inoculum. This required a very good mastery of the procedure before the inoculation was reproducible. After inoculation, 50-mm Petri dishes with colonies were placed into the housing (pre-sterilized by UV light for 30 minutes) covered by a pre-sterilized standard

Petri lid (90-mm diameter, THERMO FISHER, UK) and then sealed with petroleum jelly to prevent gas exchange.

2.2.4. Growth conditions

Colonies were incubated at 25°C (Memmert HPP 400 incubator, Schwabach) and exposed under a continuous LED light. Devices were covered with aluminum foil to prevent exposure to light for the heterotrophic cultivation (H); exposed to light at $60 \pm 10 \mu\text{mol} \cdot \text{m}^{-2} \cdot \text{s}^{-1}$ for the mixotrophic cultivation (M); and covered by aluminum foil for the first seven days (168 hours) and then removed from the device and exposed to $60 \pm 10 \mu\text{mol} \cdot \text{m}^{-2} \cdot \text{s}^{-1}$ until the end of the experiment (HM). In the latter case, colonies were cultivated under heterotrophic conditions and then changed to mixotrophic conditions. In addition, three extra hetero-mixotrophic experiments at a light intensity of $50 \pm 1 \mu\text{mol} \cdot \text{m}^{-2} \cdot \text{s}^{-1}$, $75 \pm 2 \mu\text{mol} \cdot \text{m}^{-2} \cdot \text{s}^{-1}$, and $104 \pm 5 \mu\text{mol} \cdot \text{m}^{-2} \cdot \text{s}^{-1}$ in their light stages were performed to investigate the effect of light intensity (*Mean* \pm *SD*, hereafter, mean). Gas concentrations were recorded continuously without photography in these additional experiments.

2.2.5. Three-dimensional image acquisition and analysis

Five of the ten colonies were selected randomly and observed continuously using a Zeiss Axio Zoom.V16 stereo fluorescence microscope (Carl Zeiss Microscopy GmbH, Germany) during the experiment. The microscope was equipped with an objective Apo Z 1.5× and a 63 HE filter set (BP 559–585 nm, BS 590 nm, BP 600–690 nm), which matched the natural fluorescence of the chlorophyll molecules of *C. vulgaris*. The structured light feature of the ZEISS Apotome.2 was employed to obtain 3D images. 3D fluorescent images with a resolution of $6.5 \times 6.5 \times 6.5 \mu\text{m}$ (or $6.5 \times 6.5 \times 13 \mu\text{m}$ in the cases of 9 tiles needed to cover the colony, to avoid bleaching) were acquired every day for two weeks, as detailed previously (Zhang et al., 2020). Colonies in the

additional experiments of hetero-mixotrophic and mixotrophic cultivations were measured only at the beginning and end of the experiment.

2.2.6. Gas measurement

Gas concentration was monitored using a program developed in LabVIEW. The concentration of O₂ and CO₂ were recorded every 60 seconds by percentage volume except during the periods needed for imaging. To obtain the gas production rate (source or sink term), the time-derivative of the raw signal is needed. To reduce the noise level produced by the derivation of an experimental signal, the gas evolution rate was calculated as follows:

- (1) A median filter was applied over a floating window of 121 points.
- (2) Missing data during photography were filled by linear interpolation.
- (3) The derivative of gas concentration was obtained as the best linear fit over a sliding window of 120 points.
- (4) The derivative values were subsequently removed for the interval of image grabbing, extended by 120 points on each side.
- (5) The derivative was finally converted to S.I. units to be used in the gas balance equations.

2.2.7. Dry mass per cell

The dry mass of hetero-mixotrophic colonies grown at different light intensities (50, 75, and 104 $\mu\text{mol}\cdot\text{m}^{-2}\cdot\text{s}^{-1}$) was determined at the end of the experiment (14 days). Five colonies were soaked and mixed into 5mL Milli-Q water, and 100 μL of the suspension was used to determine the average cell size (D , μm) and cell density (C , $\text{cells}\cdot\text{mL}^{-1}$) using a Beckman Coulter counter, as described previously (Zhang et al., 2020). Then, 4mL of the suspension was transferred into a 50mL tube and centrifuged at 4950g for 10min at 2°C. After discarding the supernatant and washing the pellet with 2mL Milli-Q water, the suspension was centrifuged again under the same conditions. The final pellet

was transferred to a pre-weighed aluminum dish (m_{tare}) and dried in an oven at 105°C to a constant mass (m_{tot}). All measurements were performed in duplicate using the other five colonies. The dry mass per cell (m_{cell}^{dry}) was determined as follows:

$$m_{cell}^{dry} = \frac{(m_{tot} - m_{tare}) \times 5/4}{5 \times C} \quad (1)$$

2.3. Analytical methods

2.3.1. Colony growth measurement

The 3D images were treated using a serial procedure performed by three different tools: native instructions of the Zeiss software ZEN 2.3 pro, ImageJ plugins, and an in-house code developed in MATLAB® 2019a. The image processing steps, described in detail in Zhang et al. (2020), is briefly summarized here:

- (1) Convert 3D images to optical sectioning mode by software ZEN 2.3 Pro.
- (2) Preprocess images per colony
 - a) One tile—export as a sequence of 16-bit TIFF by software ZEN 2.3 Pro.
 - b) Multiple tiles—save as TIFF per tile, stitch tiles using Grid/Collection Stitching plugin of software ImageJ (Abràmoff et al., 2004; Preibisch et al., 2009), then save as sequence of 16-bit TIFF.
- (3) Compute V , R , and H of colonies using an in-house code developed in MATLAB® 2019a.

Finally, V , R , and H were measured (Table 1), and the morphological pattern was reconstructed. Note that mixotrophic growth colonies older than 6 days were reconstructed and measured based on the assumption that the invisible colony segment would fill the same area as the colony projection. In practice, this procedure assumes that the colony after 6 days has an approximately cylindrical shape, which is confirmed by the macroscopic images of the colonies.

2.3.2. Gas balance

Our novel device allows gas concentrations to be measured throughout the experiment. The raw data requires further analysis to extract the information of interest: the source terms (production or consumption of gas) due to biological activity. These source terms were deduced from the mass balance of each gas:

$$V_{eq} \times dC_{gas}/dt = B_{gas} + L_{gas} \quad (2)$$

in which V_{eq} is the equivalent storage volume of the device, the sum of the gaseous volume and the dissolved capacity (medium volume times the effective Henry's constant), ($V_{eq} = V_{gas} + V_{medium} \times H^*$), C_{gas} the gas concentration, B_{gas} the gas productivity due to biological activity, L_{gas} the source term due to leakage and t the time. The experimental derivative of the measured concentration, the dissolved dC_{gas}/dt , was obtained as described in Section 2.2.6. The effective Henry's law constant H^* , $0.2 \text{ mol} \cdot \text{L}^{-1} \cdot \text{atm}^{-1}$, for CO_2 at pH 7 (Seinfeld and Pandis, 2016). Note that as the S.I. unit is dC_{gas}/dt ($\text{kg} \cdot \text{m}^{-3} \cdot \text{s}^{-1}$), H^* needs to be converted to a dimensionless value of 4.89 (Sander, 2015). The dissolved capacity was neglected as H^* of O_2 is 150 times smaller than for CO_2 .

L_{gas} was calculated using the leakage coefficient of the given device K , assuming a linear dependence with the driving force, the gap of gas concentration between the device C_{gas} and the environment C_{gas}^{ext} :

$$L_{gas} = K(C_{gas}^{ext} - C_{gas}) \quad (3)$$

These leakage coefficients were calibrated using data from an experiment without biological activity. To that purpose, the lid was carefully sealed with petroleum jelly, and pure nitrogen was connected through the inlet until the concentration of O_2 and CO_2 stabilized close to zero. Inlet and outlet were then clipped, and the evolution of O_2 was monitored for approximately 3 days.

We substituted the solution of Eq. 3 in Eq. 2, in which $B_{gas} = 0$, and after integration, we obtained the following evolution of concentration over time:

$$C_{O_2}^{ext} - C_{O_2} = K_0 \exp\left(-\frac{K}{V_{eq}}t\right) \quad (4)$$

In which K_0 is the integration constant. Note that the recorded original gas concentration in units of percentage volume would be converted to S.I. units of $kg \cdot m^{-3}$ before substitution into Eqs. 2–4.

For each device, the leakage coefficient was determined by fitting expression (4) to the experimental data.

When analyzing biological experiments, the reference value for the external concentration C_{gas}^{ext} has a significant effect on devices having the largest leakage coefficients. To reduce the error due to the drift of the sensor offset, its value was adjusted to obtain a net gas production equal to zero at the very beginning of the experiment, when colonies are small enough for the biological activity to be negligible. Therefore, the gas values will not be considered hereafter for a period of 0 to 48h.

2.3.3 Statistically analysis

Results were expressed as *Mean ± SD* of five replicates in the study of colony development study. Propagation of uncertainty through a mathematical process was taken into account in the statistically analysis of gas yield.

3. Results and Discussion

3.1. Specific growth rate in suspension culture

The specific growth rate of *C. vulgaris* in suspension was calculated using the exponential growth period as follows:

$$\mu_l = \frac{\Delta(\ln OD)}{\Delta t} \quad (5)$$

in which OD is the optical density of *C. vulgaris* culture at 800nm, $\Delta(\ln OD)$ the difference of the logarithm of OD between the start and end of the exponential phase and Δt is the time duration of the exponential phase.

The exponential phase started at ca. 60h after inoculation and lasted 35h under photoautotrophic conditions; started at ca. 110h and lasted 27h under mixotrophic conditions and started at ca. 120h and lasted 40h under heterotrophic conditions. The specific growth rates of *C. vulgaris*, μ_{lp} , μ_{lm} , and μ_{lh} were respectively determined to be $0.023 \pm 0.003h^{-1}$, $0.088 \pm 0.002h^{-1}$ and $0.054 \pm 0.001h^{-1}$ (*Mean \pm SD*), under photoautotrophic, mixotrophic, and heterotrophic conditions. These values are consistent with published data (Canelli et al., 2020; La et al., 2019). The sum of μ_{lp} and μ_{lh} is smaller than μ_{lm} , which is consistent with previous reports (Girard et al., 2014; Martínez and Orús, 1991).

3.2. Colony development

The increasing rate of the equivalent radius of colony g could be expressed using the difference of equivalent radius R_{t_2} and R_{t_1} divided by the time between neighboring sampling time t_2 and t_1 (Meglio et al., 2014; Warren et al., 2019):

$$g(t_1, t_2) = \frac{R_{t_2} - R_{t_1}}{t_2 - t_1} \quad (6)$$

A linear radial growth rate of $4.4 \pm 0.08\mu m \cdot h^{-1}$ was observed for heterotrophic growth conditions (Fig. 2a), consistent with previously published values (Zhang et al., 2020). The linear behavior occurs because the margin of the colony maintains optimal conditions (presence of both glucose and oxygen). Under mixotrophic conditions, colonies showed linear radial growth during the first 192h at a rate of $10.8 \pm 1.37\mu m \cdot h^{-1}$, which is approximately 2.5 times higher than the heterotrophic radial rate. This ratio is larger than the one measured in suspension (1.6), probably due to more severe

nutrient limitations in heterotrophic conditions. Subsequently, radial growth gradually decreased and almost ceased after 310 hours (Fig. 2a). Two successive linear phases were observed in the hetero-mixotrophic conditions: during the dark phase, as expected, the radial rate was similar to that of heterotrophic growth, $4.6 \pm 0.03 \mu\text{m} \cdot \text{h}^{-1}$; during the light phase, colonies showed an increased radial rate of $5.9 \pm 0.58 \mu\text{m} \cdot \text{h}^{-1}$, which is midway between heterotrophic and mixotrophic conditions.

Similar to what was observed in Zhang et al., (2020), the height of colony $Z(t)$ behaved asymptotically, regardless of the growth conditions (Fig. 2b):

$$Z(t) = Z_{max} [1 - e^{\left(\frac{-t-t_{z0}}{\tau_z}\right)}] \quad (7)$$

In which Z_{max} is the asymptotic height of the colony, t_{H0} the time shift due to the initial height of the inoculum, τ_H the characteristic time constant of height growth, and t the age of the colony. Z_{max} of colonies under heterotrophic and hetero-mixotrophic conditions were not significantly different, approximately $1230 \mu\text{m}$. For heterotrophic conditions, the limitation in height is explained by two limiting factors: diffusion of glucose upwards from the solid medium and downwards diffusion of oxygen from the surrounding gas. Mixotrophic Z_{max} was higher ($1521 \mu\text{m}$), likely because photosynthesis can occur on the top of the colony over a certain thickness due to light attenuation. Light exposure at the top of the colony induces photosynthesis, while respiration can occur at the colony margin, where oxygen and glucose are present. In addition, the core of the colony, at least up to a certain thickness, is also likely to have favorable growth conditions, with glucose provided by the solid substrate and oxygen provided by the top of the colony, where oxygen is produced by photosynthesis. Consistently, the maximum height of a colony under mixotrophic conditions was higher than other conditions as it benefits from both photosynthesis and respiration. The decrease of the growth rate in height observed at ca. 192h can be explained by the

limitation of nutrients (N, P, and other substances) needed for photosynthesis due to transportation (Warren et al., 2019). However, it is not yet clear why the radial growth is reduced and eventually stops in mixotrophic conditions, as the margin of the colony continues to benefit from the presence of oxygen and glucose.

The specific growth rate of a colony (μ_s) in terms of volume could be expressed as the difference of the logarithm volume $\Delta(\ln V)$ divided by the length of time (Δt):

$$\mu_s = \Delta(\ln V) / \Delta t \quad (8)$$

The volumetric growth of colonies gradually decreases, which can be explained by the same trend observed for the vertical growth (Fig. 2c). The mixotrophic volumetric growth rate, determined as the slope during the exponential phase (from 0 to 96 hours in this case), is larger than that of heterotrophic conditions. The colony under the light stage of hetero-mixotrophic conditions depicts a volumetric growth slightly higher than under heterotrophic, as it benefits from light after 168h. The global growth rates were determined by Eq. 8. The values of heterotrophic and mixotrophic conditions μ_{sh} and μ_{sm} were $0.025h^{-1}$ and $0.045h^{-1}$, respectively. For both, a reduction of ca. 50% was observed compared to the corresponding conditions in liquid suspension ($0.054 h^{-1}$ and $0.088 h^{-1}$). This ratio remained modest considering the limitations of nutrient migration in colonies: it seems that *C. vulgaris* can take advantage of its environment, even under constraints.

To compare one experiment using the heterotrophic conditions as a reference, the growth ratios in radius R_R (linear scale) and in volume R_V (logarithmic scale) over a given time interval $[t_1, t_2]$, were introduced:

$$R_R(t_1, t_2) = \frac{g'}{g} = \frac{R'_{t_2} - R'_{t_1}}{R_{t_2} - R_{t_1}} \quad (9)$$

$$R_V(t_1, t_2) = \frac{\mu'_s}{\mu_s} = \frac{\ln V'_{t_2} - \ln V'_{t_1}}{\ln V_{t_2} - \ln V_{t_1}} \quad (10)$$

In Fig. 2d, the growth ratios were computed using the two neighboring instants in Eqs. 9 and 10: $t_1 = t_{i-1}$ and $t_2 = t_{i+1}$ for the values computed at t_i . Consistently, R_R and R_V remained close to the unit during the dark stage of the hetero-mixotrophic conditions. Then, the presence of light boosted the radial and volume growth by a similar factor of approximately 1.5. Under mixotrophic conditions, the radial growth rate was much larger (a factor 2.5) for ca. 150h. The ratio then decreased and eventually was only half that of the reference configuration, confirming objectively the substantial decrease in radial growth observed at the end of the experiment under mixotrophic conditions. The same trend was observed for the volumetric growth, but with smaller values explained by the log scale used for the volume values.

3.3. Oxygen and carbon dioxide production/consumption rate

Ten *C. vulgaris* colonies were grown per device under heterotrophic, hetero-mixotrophic, and mixotrophic conditions, and their gas concentration variations are shown in Fig. 3a. Under heterotrophic conditions, the concentration of O₂ decreased from 21% to 8%, and the concentration of CO₂ increased from 0% to 5% (only results with low-leakage devices are presented). Under hetero-mixotrophic conditions, the concentration of O₂ in the dark phase decreased in the same regular pattern as under heterotrophic conditions in the same period, while the decreasing rate slowed down once the light was turned on. A similar increase in CO₂ under heterotrophic cultivation was shown in the dark stage, and the increasing slope reduced once the culture was exposed to light. Under mixotrophic conditions, the concentration of O₂ decreased until 144h and then began to increase above the atmospheric concentration. After 297h, the oxygen concentration declined back to the initial value. The concentration of CO₂ increased continuously, but, surprisingly, a synchronized effect was observed (the trough depicted at ca. 267h). This unexpected wave was observed again in another two additional experiments (data not shown). It might be induced by the rhythm of the

organism, or it could also be explained by a change in colony strategy, with the establishment of synergy between respiration and photosynthesis. This notable feature merits further investigation. Furthermore, the concentration of O₂ dropped during the dark periods imposed during imaging, which is explained by the consumption of O₂ by respiration.

The biological source terms of O₂ and CO₂, calculated using Eq. 2 are depicted in Fig. 3b. In the case of heterotrophic cultivation, the O₂ consumption rate and CO₂ production rate gradually increased up to $1.3 \times 10^{-11} \text{ kg/s}$ and $1.5 \times 10^{-11} \text{ kg/s}$, respectively. These values are consistent with those of colony development over time. In the dark stage of hetero-mixotrophic cultivation, the O₂ consumption rate exhibited the same regular increase, as up to that point, the conditions were the same as in the heterotrophic cultivation. On the contrary, while in the light stage, the O₂ consumption rate and CO₂ production rate respectively stabilized around $8 \times 10^{-12} \text{ kg/s}$ and $5 \times 10^{-12} \text{ kg/s}$ despite the colony growth. In mixotrophic cultivation, O₂ was consumed during the first 134h, then oscillated around zero, and finally became positive, with a net production. The CO₂ production was similar to the other two modes up to 134h, then oscillated around $6 \times 10^{-12} \text{ kg/s}$ with a larger amplitude than O₂. It then increased rapidly and became much greater than that of the other cultures. To analyze this trend, we recall that the final dry mass of the mixotrophic colony was 4 times larger than that of the heterotrophic colony. The wave-like shape observed in the mixotrophic raw data revealed clear opposite trends in CO₂ and O₂ production rates. The decreasing portion of the CO₂ curve is missing because its concentration was outside the range of the sensor.

To understand the impact of light intensity on colony behavior, three extra hetero-mixotrophic cultivation experiments were performed with light intensities of $50 \mu\text{mol} \cdot \text{m}^{-2} \cdot \text{s}^{-1}$, $75 \mu\text{mol} \cdot \text{m}^{-2} \cdot \text{s}^{-1}$, and $104 \mu\text{mol} \cdot \text{m}^{-2} \cdot \text{s}^{-1}$ during the light stage (Fig. 3c).

Their gas production rates were obtained using Eq. 2 (Fig.3d). Consistent with the previous experiments, the rates of O₂ consumption and CO₂ production increased during the dark stage, after which the three cases showed different behaviors. Sharp variation rates of O₂ consumption and CO₂ production rate were observed 24h after light exposure, namely 169 to 192h, indicating that the colony metabolic pathway changed suddenly, namely, that photosynthesis started due to light exposure. This is not surprising as the metabolism in mixotrophic mode depends on light intensity: the stronger the light, the deeper it penetrates the colony, which induces higher photosynthesis and a shape variation. After 192h, the gas production behavior was different at the three light intensities. At the intensity of $50\mu\text{mol} \cdot \text{m}^{-2} \cdot \text{s}^{-1}$, the rate of O₂ consumption and CO₂ production continued the same trend as observed in the dark stage until 264h, then it stabilized until the end. At $75\mu\text{mol} \cdot \text{m}^{-2} \cdot \text{s}^{-1}$, O₂ consumption rate slightly decreased with the colony growth and stabilized at zero until the end of the experiment. The CO₂ production rate increased then oscillated in the range of zero to $1.0 \times 10^{-11} \text{ kg/s}$. At $104\mu\text{mol} \cdot \text{m}^{-2} \cdot \text{s}^{-1}$, O₂ consumption rate decreased rapidly to zero at 250h, and eventually became positive (net production of O₂). The CO₂ production rate was similar to that of $104\mu\text{mol} \cdot \text{m}^{-2} \cdot \text{s}^{-1}$ but $4 \times 10^{-12} \text{ kg/s}$ smaller after 192h. The evolution of gas production of these three experiments tells us that photosynthesis and respiration always occurred in synergy inside the colony in the mixotrophic mode. Finally, to understand the time evolution of gas production during the light exposure phase, we recall that the colony height evolved from 600μm to roughly 1000μm during this phase, which indicates that the fraction of the colony exposed to light was significantly reduced.

3.4. Gas yields during different trophic modes

The raw data were further analyzed, together with the biomass production, to obtain the stoichiometric balances and indicators of gas yields (mass of biomass produced per mass of produced or consumed gas).

Initially, the source terms of gas were integrated to obtain the net mass of gas produced, or consumed, over a given time interval:

$$m_{gas}(t_1, t_2) = \sum_{i=1}^{T-1} \frac{B_{gas}(i) + B_{gas}(i+1)}{2} \times (t_{i+1} - t_i) \quad (11)$$

in which T is the sampling number of gas source between t_1 and t_2 and B_{gas} the biology-based O_2 consumption or CO_2 production.

Similarly, the number of cells in the colony at any time t , $N(t)$, is determined using the colony volume $V(t)$ at time t , the average cell diameter D , and the packing factor ω :

$$N(t) = \frac{V(t) \times \omega}{3/4 \times \pi \times (D/2)^3} \quad (12)$$

The gas yields, Y_{O_2} and Y_{CO_2} , are defined as the mass of gas produced per dry biomass (g gas/g cell). Negative values represent gas consumption and positive values, gas production. The gas yields can then be computed for any two times at which the colony volume is available:

$$Y_{gas}(t_1, t_2) = \frac{m_{gas}(t_1, t_2)/N_{col}}{m_{cell}^{dry} \times (N(t_2) - N(t_1))} \quad (13)$$

in which t_1 and t_2 are any two imaging times, N_{col} the number of colonies (equal to 10 in this case), $N(t_1)$ and $N(t_2)$ respectively, the number of cells in the colony at time t_1 and t_2 , and m_{cell}^{dry} the dry mass of a single cell as calculated by Eq. 1 (Table 2). It is worth noting that m_{cell}^{dry} of hetero-mixotrophic cultivation slightly increased with light intensity, which is consistent with previous reports (Deng et al., 2019; Li et al., 2014).

The evolution of the gas yields is depicted in Fig. 4. **The error bars of Y_{gas} were**

obtained by considering the error propagation from the standard deviation of the dry mass of a colony and a $\pm 5\%$ error in the gas leakage. Total relative error was calculated as the sum of relative error and then converted to absolute error.

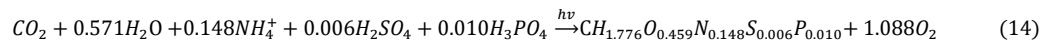
In heterotrophic mode, the average Y_{O_2} was approximately $-0.64\text{g O}_2/\text{g cell}$ and Y_{CO_2} approximately $0.78\text{g CO}_2/\text{g cell}$. This indicates that 0.32g CO_2 were produced to form 1g dry biomass, and 0.78g O_2 were consumed in the interim. During the dark stage of the hetero-mixotrophic mode, Y_{O_2} increased from -0.22 to -0.75g cell/g O_2 and Y_{CO_2} increased from 0.03 to 0.70g cell/g CO_2 . As expected, these values were close to those of heterotrophic conditions. During the light stage, after 168h, Y_{O_2} and Y_{CO_2} stabilized at approximately -0.3g cell/g O_2 and 0.3g cell/g CO_2 , respectively. Compared to the heterotrophic mode, the effect of light on the gas yield is therefore clearly discerned from 168h onwards: i) regular decrease of Y_{O_2} for the light stage of hetero-mixotrophic cultivation instead of a regular increase of Y_{O_2} , consistent with the colony growth for heterotrophic, and ii) halved Y_{CO_2} , stabilized at a low level for the light stage of hetero-mixotrophic cultivation instead of rapidly increasing with the colony size for heterotrophic. In mixotrophic mode, the increased production of CO_2 at the end suggests that the heterotrophic portion increased due to the volume of colony growth.

Under most conditions, the gas yields evolved rapidly at the beginning of the culture, during which the colonies were very small, and then stabilized. It is, therefore, reasonable to analyze the average yields over more extended periods, computed as a weighted average (ratio of the sum of masses). We computed these averaged values over the entire cultivation duration of 336h in the case of constant conditions and split the time interval into two stages (dark stage and light stage) in the case of hetero-mixotrophic conditions (Table. 3).

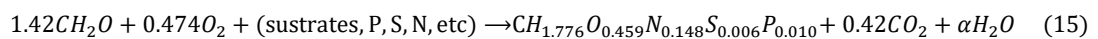
The Y_{O_2} in heterotrophic mode was in the range of -0.43 to -0.72 g O_2 /g cell. The increase in Y_{O_2} with the light intensity in hetero-mixotrophic cultivation coincided with the increase in photosynthesis partly because of the deeper light penetration. The positive signs of both Y_{O_2} and Y_{CO_2} in the mixotrophic cultivation indicates that the metabolism of the colony is more complex and does not merely consist of photosynthesis and respiration. It will be discussed in the next section.

3.5. Metabolism of the colony in different trophic modes

To further understand the metabolism inside the colony, we consider two main growth modes: photosynthetic and heterotrophic. The stoichiometric equation of photosynthesis was from Hadj-Romdhane et al. (2012):



The heterotrophic growth mode consists mainly of respiration. However, fermentation, a slower and less efficient metabolism than respiration in the case of algae (Syrett and Wong, 1963), is certainly non-negligible in the case of the colony as large parts lack oxygen. The stoichiometric balance of the heterotrophic growth was derived from our experimental data to account for both respiration and fermentation (Table 3). In this equation, the molar coefficients of O_2 and CO_2 were defined to obtain the gas yields measured in heterotrophic cultivation (-0.64 g O_2 /g cell and 0.78 g CO_2 /g cell). The chemical composition of *C. vulgaris* was obtained from Hadj-Romdhane et al. (2012), which neglects the difference between cultivation and respecting the carbon balance. The coefficient of glucose was computed to close the carbon balance. The global chemical process of heterotrophic growth of *C. vulgaris* is finally summarized as:



The coefficient of water is not specified as it is not the aim of this work. The cell yield on the organic carbon source (glucose) was 0.56g cell/g glucose, within the range of our previous report (Zhang et al., 2020), supporting this approach.

Equations 14 and 15 allow the theoretical gas yields to be computed (Fig. 5). Using these theoretical values, the proportion of heterotrophy and photosynthesis was fitted to obtain the measured yield of O₂ and CO₂ under the light stages of the heteromixotrophic experiments at different light intensities. The photosynthesis proportions were 16% , 28% , and 31% for 50, 75, and 104 $\mu\text{mol} \cdot \text{m}^{-2} \cdot \text{s}^{-1}$, respectively. Comparison of the measured gas yields with the ones predicted using the theoretical values and the identified photosynthesis ratios remain consistent: i) for O₂, theoretical values of -0.30, -0.05, and 0.014g O₂/g cell compared to measured values of -0.34, -0.04, and 0.001g O₂/g cell, respectively, for 50, 75, and 104 $\mu\text{mol} \cdot \text{m}^{-2} \cdot \text{s}^{-1}$; ii) for CO₂, theoretical values of 0.36, 0.04, and -0.04g CO₂/g cell compared to measured values of 0.31, 0.04, and -0.04g CO₂/g cell respectively for 50, 75, and 104 $\mu\text{mol} \cdot \text{m}^{-2} \cdot \text{s}^{-1}$. As expected, the photosynthesis portion increased with light intensity, but not linearly. The highest light intensity was less efficient. **Cultures may have entered the photo-inhibition domain.** Contrary to cultures in suspension, cells are static in immobilized cultures and cannot benefit from auto-shading once exposed to light (Pozzobon and Perré, 2018). **However, this is unlikely at this moderate light intensity. Another explanation could be the limitation of gas transfer needed for the synergy between the heterotrophic and photosynthesis zones (O₂ produced by photosynthesis provided to the bottom of the colony and CO₂ produced by respiration likely to supply the photosynthesis layer).**

Photosynthesis occurs on the top of the colony under a decreased light intensity with depth. Using the classical Beer-Lambert law for the light attenuation, the light profile from the top could be obtained by the following expression:

$$I = I_0 e^{-\rho b h} \quad (16)$$

in which I_0 is the incident light, h the distance to the surface of the colony, $\rho (= \frac{m_{\text{cell}}^{\text{dry}} \times \omega}{3/4 \times \pi \times (D/2)^3})$, $m_{\text{cell}}^{\text{dry}}$ is cell dry biomass, ω the packing density, and D the diameter of the cell) the colony density, approximately 220g/L in our case, and b the attenuation coefficient. With an extinction coefficient b of $143 \text{ L} \cdot \text{g}^{-1} \cdot \text{m}^{-1}$ (La et al., 2019; Vergara et al., 2016) the characteristic attenuation length equals $32 \mu\text{m}$. Assuming a light compensation point at $5 \mu\text{mol} \cdot \text{m}^{-2} \cdot \text{s}^{-1}$ (Shiraiwa and Miyachi, 1983), the colony thickness likely to ensure photosynthesis was determined to be $73 \mu\text{m}$, $86 \mu\text{m}$, and $96 \mu\text{m}$, respectively, at light intensities I_0 of 50, 75, and $104 \mu\text{mol} \cdot \text{m}^{-2} \cdot \text{s}^{-1}$. **These values confirm that the heterotrophic thickness is much larger than the photosynthesis layer, which supports the assumption of gas transfer limitation.**

These global proportions of different metabolic pathways obtained through our detailed analysis of gas measurements allow for a detailed analysis of synergy within the colony.

A globally spherical cap pattern was conserved during the entire experiment only for heterotrophic conditions (Fig. 6a left), consistent to what has been reported previously (Zhang et al., 2020). In this case, both nutrients and oxygen remained abundant at the margin of the colony, an optimal growth conditions for cells, which explains the constant radial growth. In contrast, growth conditions worsened where the colony is thicker, due to the cross-diffusion of oxygen from the top and glucose from the bottom, together with the sink terms due to the biological activity (Fig. 6b left).

Schematic glucose and oxygen profiles at the center of the colony reflect both diffusion and consumption within the colony.

For mixotrophic conditions, the radial growth was initially very fast, due to this efficient mode, but significantly reduces over time and finally almost stopped, even though the growth in height continued. This balance between radial and height growth necessarily changes the colony shape, which becomes more cylindrical (Fig. 6a middle). It might be explained by an optimization of resources and a specialization of cells: photosynthesis on the top, where light is present, and heterotrophy at the bottom, where glucose is present. Oxygen provided by photosynthesis is likely to diffuse downwards to supply oxygen to heterotrophic zone (Fig. 6b right). Consequently, the oxygen profile decreases less rapidly than in heterotrophic conditions. A synergy between photosynthesis and heterotrophy occurs also for CO₂, as the CO₂ consumption in the photosynthesis, together with the CO₂ production in the heterotrophic zone, generates a gradient that activates its diffusion towards the top of the colony. In the meantime, wrinkles appear at the surface. Those structures developing in the presence of light are likely to allow more cells to access both oxygen and light, which was also reported in a bacterial biofilm (Dietrich et al., 2013; Jo et al., 2017). Under hetero-mixotrophic conditions, the spherical cap shape was lost at 216h, approximately 50h after the light had been turned on (168h) (Fig. 6a right), which shows a tendency to be cylindrical.

There is another possible explanation for why radial growth stops in the presence of light: top cells are likely to protect the bottom cells from light, potentially playing a role in the inhibition of the heterotrophic pathway.

4. Conclusions

An original culture device, designed and manufactured in-house, was used to continuously assess the gas and biomass production. The gas balance of immobilized *C. vulgaris* during different trophic modes was achieved. The cultivation mode affected

both the biomass growth rate and morphology of the colony, indicating the different metabolic reactions occurred in the colony. In the mixotrophic cultivation mode, the proportion of photosynthesis increased with light intensity, but the dependence was not linear, which reveals a limiting factor that might be gas transfer inside the colony. Synergistic mechanisms within the colony was proposed for both heterotrophic and mixotrophic conditions.

E-supplementary data of this work can be found in online version of the paper.

Acknowledgments

This study was conducted in the Centre Européen de Biotechnologie et de Bioéconomie (CEBB), supported by Région Grand Est, Département de la Marne, Grand Reims and the European Union. In particular, the authors would like to thank the Département de la Marne for its financial support. The authors thank Mahamadou Mounkaila of LGPM for assistance in setting up the gas sensing system, and Joel Casalinho of LGPM for the inspiration of the design of the culture device.

References

1. Abràmoff, M.D., Magalhães, P.J., Ram, S.J., 2004. Image processing with ImageJ. *Biophotonics Int.* 11, 36–42.
2. Amit, Ghosh, U.K., 2019. Utilization of kinnow peel extract with different wastewaters for cultivation of microalgae for potential biodiesel production. *J. Environ. Chem. Eng.* 7, 103135.
3. Amit, Nayak, J.K., Ghosh, U.K., 2020. Microalgal remediation of anaerobic pretreated pharmaceutical wastewater for sustainable biodiesel production and electricity generation. *J. Water Process Eng.* 35, 101192.
4. Ayed, H.B.A. Ben, Taidi, B., Ayadi, H., Pareau, D., Stambouli, M., 2017. The use of *Chlorella vulgaris* to accumulate magnesium under different culture conditions. *J. Appl. Biotechnol. Bioeng.* 2, 43–48.

5. Bernard, O., Lopes, F., Pruvost, E., Sciandra, A., 2018. Method and unit for producing microalgae. U.S. Patent 10,106,765.
6. Blanken, W., Janssen, M., Cuaresma, M., Libor, Z., Bhaiji, T., Wijffels, R.H., 2014. Biofilm growth of *Chlorella sorokiniana* in a rotating biological contactor based photobioreactor. *Biotechnol. Bioeng.* 111, 2436–2445.
7. Canelli, G., Neutsch, L., Carpine, R., Tevere, S., Giuffrida, F., Rohfritsch, Z., Dionisi, F., Bolten, C.J., Mathys, A., 2020. *Chlorella vulgaris* in a heterotrophic bioprocess: Study of the lipid bioaccessibility and oxidative stability. *Algal Res.* 45.
8. Cardol, P., Forti, G., Finazzi, G., 2011. Regulation of electron transport in microalgae. *Biochim. Biophys. Acta - Bioenerg.* 1807, 912–918.
9. Chojnacka, K., Marquez-Rocha, F.-J., 2004. Kinetic and stoichiometric relationships of the energy and carbon metabolism in the culture of microalgae. *Biotechnology* 3, 21–34.
10. Clément-Larosière, B., Lopes, F., Gonçalves, A., Taidi, B., Benedetti, M., Minier, M., Pareau, D., 2014. Carbon dioxide biofixation by *Chlorella vulgaris* at different CO₂ concentrations and light intensities. *Eng. Life Sci.* 14, 509–519.
11. Cournac, L., Latouche, G., Cerovic, Z., Redding, K., Ravenel, J., Peltier, G., 2002. In vivo interactions between photosynthesis, mitorespiration, and chlororespiration in *Chlamydomonas reinhardtii*. *Plant Physiol.* 129, 1921–1928.
12. Darvehei, P., Bahri, P.A., Moheimani, N.R., 2018. Model development for the growth of microalgae: A review. *Renew. Sustain. Energy Rev.* 97, 233–258.
13. Deng, X., Chen, B., Xue, C., Li, D., Hu, X., Gao, K., 2019. Biomass production and biochemical profiles of a freshwater microalga *Chlorella kessleri* in mixotrophic culture: Effects of light intensity and photoperiodicity. *Bioresour. Technol.* 273, 358–367.
14. Dietrich, L.E.P., Okegbe, C., Price-Whelan, A., Sakhtah, H., Hunter, R.C., Newmana, D.K., 2013. Bacterial community morphogenesis is intimately linked to the intracellular redox state. *J. Bacteriol.* 195, 1371–1380.

15. Girard, J.M., Roy, M.L., Hafsa, M. Ben, Gagnon, J., Faucheux, N., Heitz, M., Tremblay, R., Deschênes, J.S., 2014. Mixotrophic cultivation of green microalgae *Scenedesmus obliquus* on cheese whey permeate for biodiesel production. *Algal Res.* 5, 241–248.
16. Gouveia, L., 2007. Biodiesel from microalgae. *Biotechnol. Adv.* 25, 294–306.
17. Hadj-Romdhane, F., Jaouen, P., Pruvost, J., Grizeau, D., Van Vooren, G., Bourseau, P., 2012. Development and validation of a minimal growth medium for recycling *Chlorella vulgaris* culture. *Bioresour. Technol.* 123, 366–374.
18. Han, B.P., 2001. Photosynthesis-Irradiance response at physiological level: A mechanistic model. *J. Theor. Biol.* 213, 121–127.
19. Hu, J., Nagarajan, D., Zhang, Q., Chang, J.S., Lee, D.J., 2018. Heterotrophic cultivation of microalgae for pigment production: A review. *Biotechnol. Adv.* 36, 54–67.
20. IPCC, 2019. “Global Warming of 1.5 °C”. <https://www.ipcc.ch/sr15/>
21. Jo, J., Cortez, K.L., Cornell, W.C., Price-whelan, A., Lars, E.P., 2017. An orphan cbb3-type cytochrome oxidase subunit supports *Pseudomonas aeruginosa* biofilm growth and virulence. *eLife* 6, e30205.
22. Kong, W., Song, H., Cao, Y., Yang, H., Hua, S., Xia, C., 2011. The characteristics of biomass production, lipid accumulation and chlorophyll biosynthesis of *Chlorella vulgaris* under mixotrophic cultivation. *African J. Biotechnol.* 10, 11620–11630.
23. Kromkamp, J.C., Peene, J., 2001. Oxygen consumption in the light by unicellular algae. In *Proceedings 12th International Congress on Photosynthesis Brisbane, Australia*, 1 – 6.
24. La, A., Perré, P., Taidi, B., 2019. Process for symbiotic culture of *Saccharomyces cerevisiae* and *Chlorella vulgaris* for in situ CO₂ mitigation. *Appl. Microbiol. Biotechnol.* 103, 731–745.
25. Lewitus, A.J., Kana, T.M., 1995. Light respiration in six estuarine phytoplankton species: contrasts under photoautotrophic and mixotrophic growth conditions. *J. Phycol.* 31, 754–761.
26. Li, T., Zheng, Y., Yu, L., Chen, S., 2014. Mixotrophic cultivation of a *Chlorella sorokiniana* strain for enhanced biomass and lipid production. *Biomass and Bioenergy* 66, 204–213.

27. Manhaeghe, D., Michels, S., Rousseau, D.P.L., Van Hulle, S.W.H., 2019. A semi-mechanistic model describing the influence of light and temperature on the respiration and photosynthetic growth of *Chlorella vulgaris*. *Bioresour. Technol.* 274, 361–370.
28. Martínez, F., Orús, M.I., 1991. Interactions between glucose and inorganic carbon metabolism in *Chlorella vulgaris* strain UAM 101. *Plant Physiol.* 95, 1150–1155.
29. Meglio, J. Di, Lindner, A.B., Daerr, A., Murray, A., Hersen, P., 2014. Growing yeast into cylindrical colonies. *Biophys. J.* 106, 2214–2221.
30. Mohammad Mirzaie, M.A., Kalbasi, M., Mousavi, S.M., Ghobadian, B., 2016. Investigation of mixotrophic, heterotrophic, and autotrophic growth of *Chlorella vulgaris* under agricultural waste medium. *Prep. Biochem. Biotechnol.* 46, 150–156.
31. Mohan, S.V., Rohit, M.V., Subhash, G.V., Chandra, R., Devi, M.P., Butti, S.K., Rajesh, K., 2019. Algal oils as biodiesel, Second Edi. ed, *Biofuels from Algae*. Elsevier B.V.
32. Molina, E., Fernández, J., Acién, F.G., Chisti, Y., 2001. Tubular photobioreactor design for algal cultures. *J. Biotechnol.* 92, 113–131.
33. Ogonna, J.C., Ichige, E., Tanaka, H., 2002. Interactions between photoautotrophic and heterotrophic metabolism in photoheterotrophic cultures of *Euglena gracilis*. *Appl. Microbiol. Biotechnol.* 58, 532–538.
34. Patino, R., Janssen, M., von Stockar, U., 2007. A study of the growth for the microalga *Chlorella vulgaris* by photo-bio-calorimetry and other on-line and off-line techniques. *Biotechnol. Bioeng.* 96, 757–767.
35. Perez-Garcia, O., Bashan, Y., 2015. Microalgal heterotrophic and mixotrophic culturing for bio-refining: from metabolic routes to techno-economics, in: *Algal Biorefineries*. Springer, pp. 61–131.
36. Pozzobon, V., Perré, P., 2018. Han's model parameters for microalgae grown under intermittent illumination: Determined using particle swarm optimization. *J. Theor. Biol.* 437, 29–35.
37. Preibisch, S., Saalfeld, S., Tomancak, P., 2009. Globally optimal stitching of tiled 3D

- microscopic image acquisitions. *Bioinformatics* 25, 1463–1465.
38. Rattanapoltee, P., Kaewkannetra, P., 2014. Cultivation of microalga, *Chlorella vulgaris* under different auto-hetero-mixo trophic growths as a raw material during biodiesel production and cost evaluation. *Energy* 78, 4–8.
 39. Rincon, S.M., Romero, H.M., Aframehr, W.M., Beyenal, H., 2017. Biomass production in *Chlorella vulgaris* biofilm cultivated under mixotrophic growth conditions. *Algal Res.* 26, 153–160.
 40. Sa, C., Zebib, B., Merah, O., Pontalier, P.Y., Vaca-Garcia, C., 2014. Morphology , composition , production , processing and applications of *Chlorella vulgaris*: A review. *Renew. Sustain. Energy Rev.* 35, 265–278.
 41. Sander, R., 2015. Compilation of Henry’s law constants (version 4.0) for water as solvent. *Atmos. Chem. Phys.* 15, 4399–4981.
 42. Schnurr, P.J., Espie, G.S., Allen, D.G., 2014. The effect of light direction and suspended cell concentrations on algal biofilm growth rates. *Appl. Microbiol. Biotechnol.* 98, 8553–8562.
 43. Seinfeld, J.H., Pandis, S.N., 2016. Atmospheric chemistry and physics: from air pollution to climate change, Second. ed. John Wiley & Sons, Hoboken, NJ.
 44. Shiraiwa, Y., Miyachi, S., 1983. Factors controlling induction of carbonic anhydrase and efficiency of photosynthesis in *Chlorella vulgaris* llh cells. *Plant Cell Physiol.* 24, 919–923.
 45. Shoener, B.D., Schramm, S.M., Béline, F., Bernard, O., Martínez, C., Plósz, B.G., Snowling, S., Steyer, J.-P.P., Valverde-Pérez, B., Wágner, D., Guest, J.S., 2019. Microalgae and cyanobacteria modeling in water resource recovery facilities: A critical review. *Water Res.* X 2, 100024.
 46. Syrett, P., Wong, H., 1963. The Fermentation of glucose by *Chlorella vulgaris*. *Biochem. J.* 89, 308–315.
 47. Tang, T., Fadaei, H., Hu, Z., 2014. Rapid evaluation of algal and cyanobacterial activities through specific oxygen production rate measurement. *Ecol. Eng.* 73, 439–445.
 48. Vergara, C., Muñoz, R., Campos, J.L., Seeger, M., Jeison, D., 2016. Influence of light intensity

- on bacterial nitrifying activity in algal-bacterial photobioreactors and its implications for microalgae-based wastewater treatment. *Int. Biodeterior. Biodegrad.* 114, 116–121.
49. Warren, M.R., Sun, H., Yan, Y., Cremer, J., Li, B., Hwa, T., 2019. Spatiotemporal establishment of dense bacterial colonies growing on hard agar. *elife* 8, 1–47.
50. Zhang, J., Tran, T.-B.-T., Taidi, B., Lu, P., Perré, P., 2020. *Chlorella vulgaris* heterotrophic colony development and interaction. *Algal Res.* 49, 101907.

Figure Captions

Fig. 1. In-house culture device designed to monitor *in situ* gas concentration.

Fig. 2. *Chlorella vulgaris* colony development.

Fig. 3. Gas concentration variation in heterotrophic, hetero-mixotrophic, and mixotrophic modes (a) and their gas production rates (b). Gas concentration variation in hetero-mixotrophic conditions with light intensities of $50\mu\text{mol} \cdot \text{m}^{-2} \cdot \text{s}^{-1}$, $75\mu\text{mol} \cdot \text{m}^{-2} \cdot \text{s}^{-1}$, and $104\mu\text{mol} \cdot \text{m}^{-2} \cdot \text{s}^{-1}$ at light stage (c) and their gas production rates (d). The concentration of O₂ and CO₂ are represented by blue and red lines, respectively. The green lines represent the “light on” moment in the hetero-mixotrophic cultivation experiment. Missing periods of lines in graph (a) and (b) are the duration of photography.

Fig. 4. Evolution of gas yield of *C. vulgaris* in different trophic modes. (a) and (b) in heterotrophic mode. (c) and (d) in hetero-mixotrophic mode, with the light switched on at 168h. (e) and (f) in mixotrophic mode.

Fig. 5. Proportions of photosynthesis, the complement to 100% being heterotrophic growth as a function of light intensity deduced from the experimental yield of O₂ and CO₂. Theoretical gas yield determined for O₂ and CO₂ using the stoichiometric Eqs. 14 and 15.

Fig. 6. (a) Photos of colony morphology under heterotrophic (left, 142h), mixotrophic (middle, 142h), and hetero-mixotrophic (right, 216h) cultivation modes. The light was switched on at 168h for the hetero-mixotrophic cultivation mode. Scale bar, 1mm. (b) A synthetic diagram of the microenvironment of the colony, metabolism of the colony with and without light. The profiles of growth conditions exhibit the synergies inside the colony.

Table 1. Objective variables determined on colonies by 3D image processing.

Table 2. Colony characteristics.

Table 3. Gas yield of *C. vulgaris* in different trophic modes.

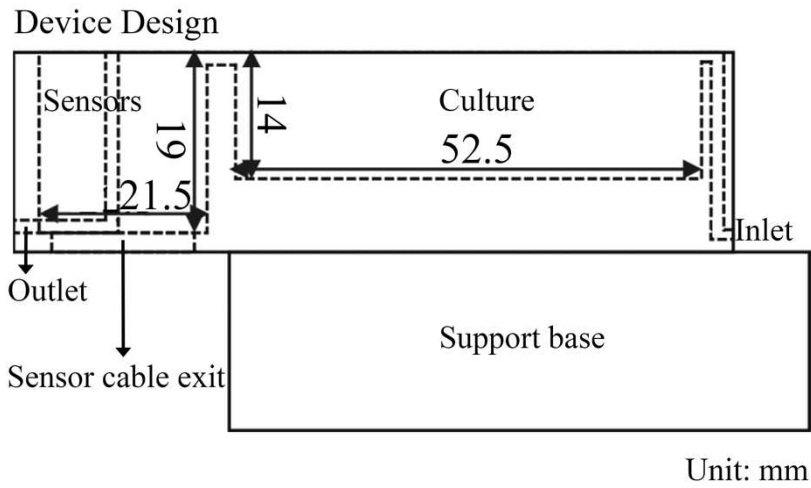
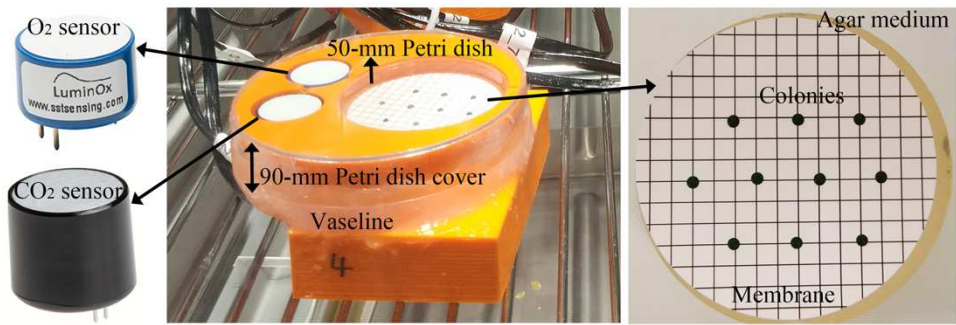


Fig. 1.

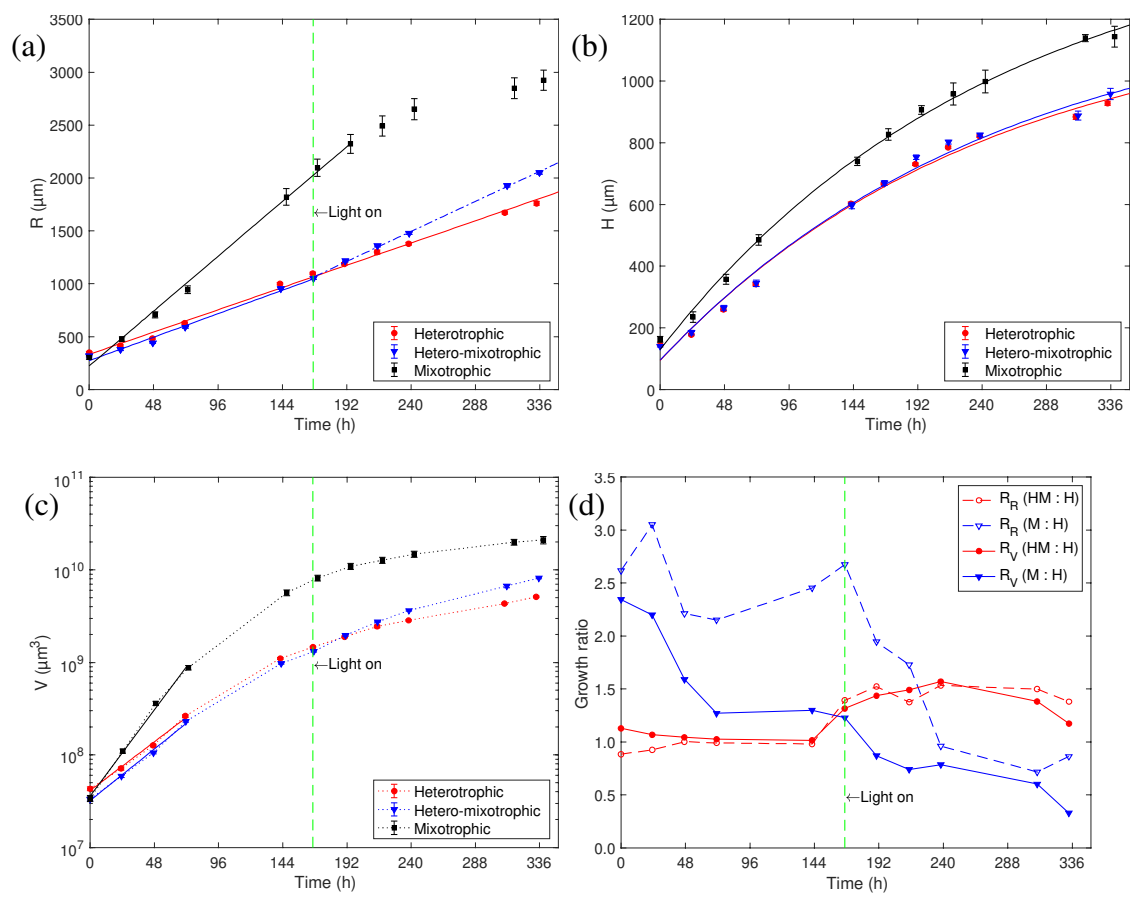


Fig. 2.

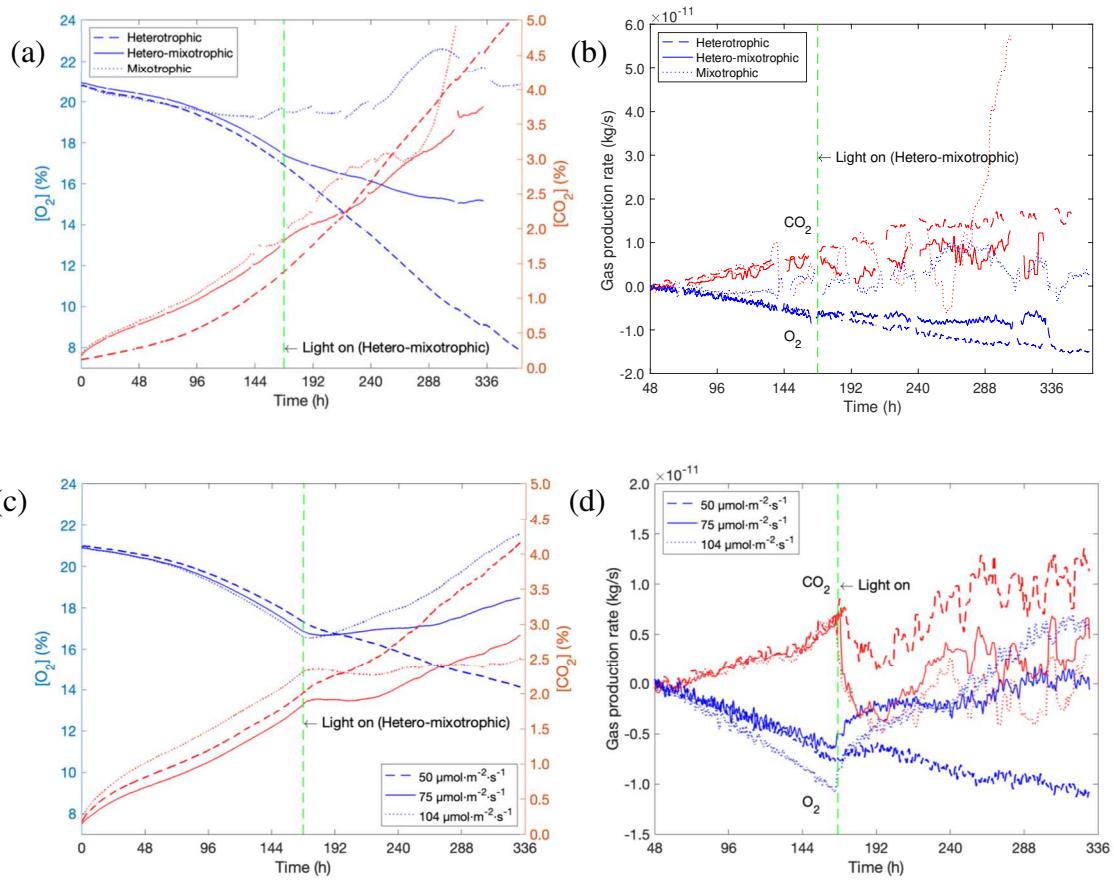


Fig. 3.

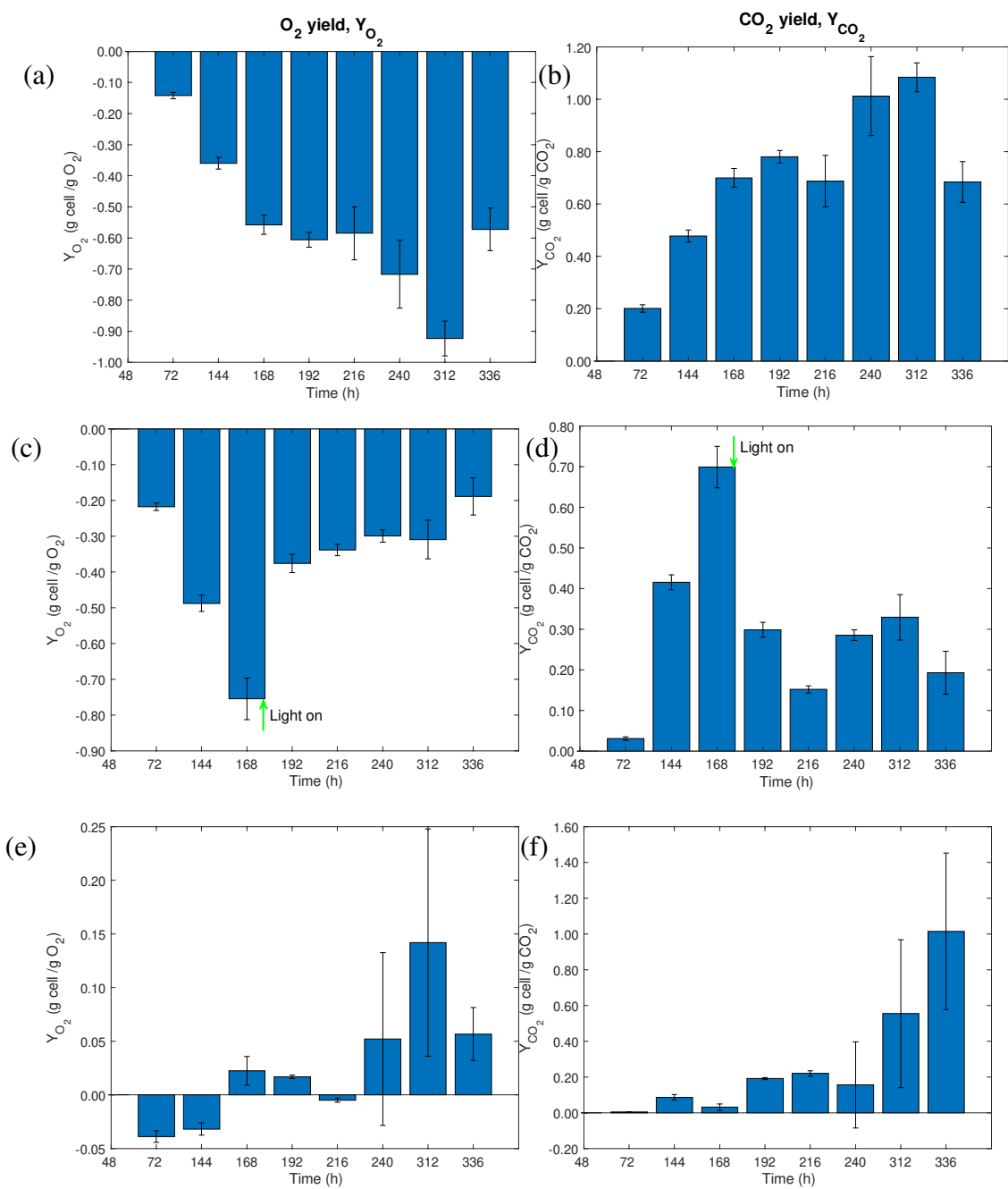


Fig. 4.

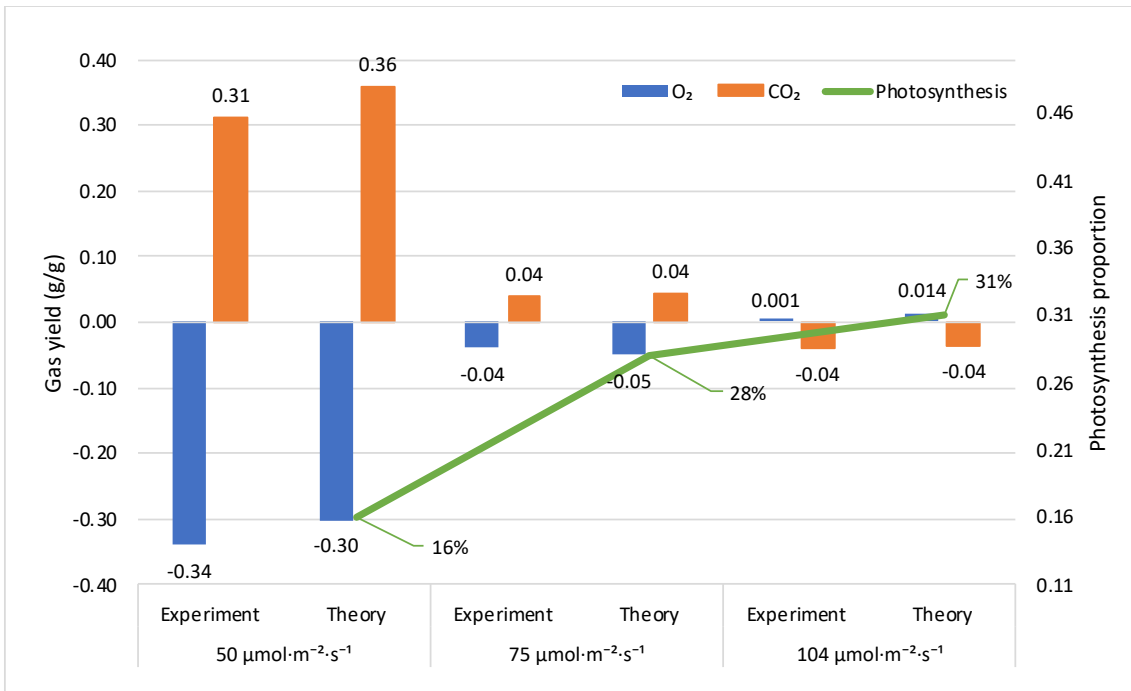
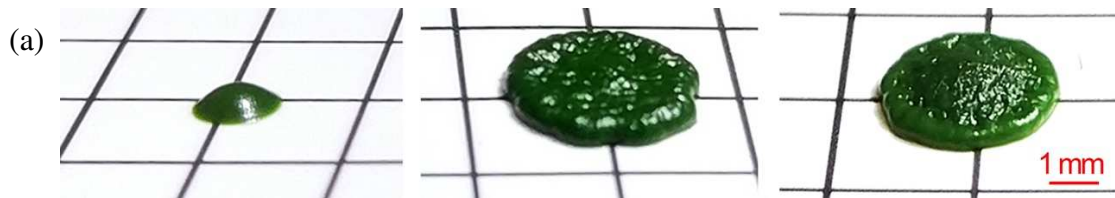


Fig. 5.



(b)

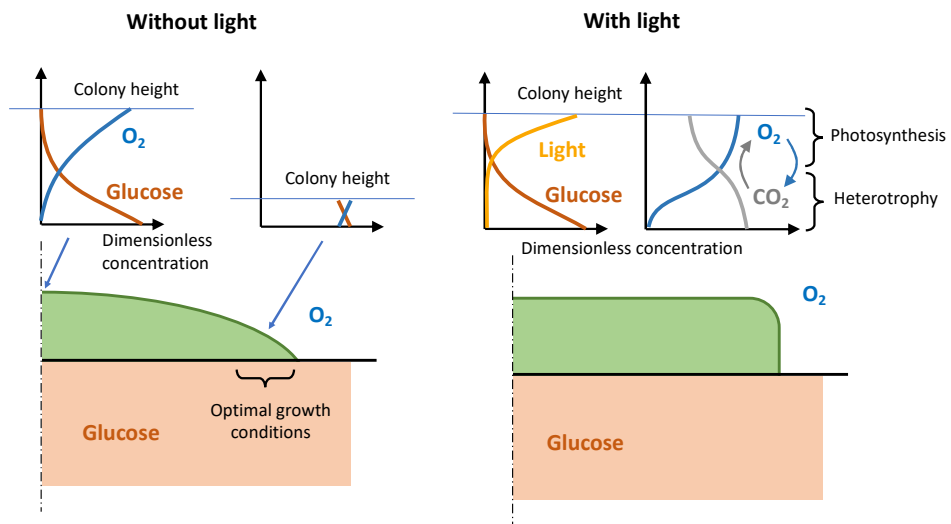


Fig. 6.

Table 1.

Features	Calculation	Definition
V	$V = \sum_x \sum_y P_{x,y} \times \Delta x \times \Delta y$ <p>$P_{x,y}$ is the value of height at position (x, y), Δx and Δy are the pixel sizes.</p>	Colony volume computed as the discrete sum of elementary columns.
R	$R = \sqrt{A_p/\pi}$ <p>A_p represents the area of the colony projection.</p>	Equivalent radius of the colony
H	$H = (N_t - N_b) \times \Delta z$ <p>where N_t and N_b are respectively the number of top and bottom slice, and Δz is the interval between neighbor slices.</p>	Height is the distance between the first and last visible slices.

Table 2.

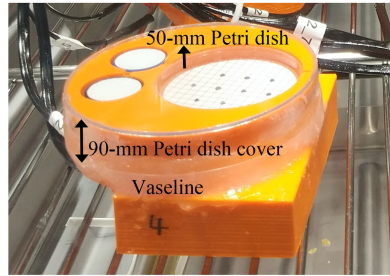
Parameter (unit)	Value (Mean \pm SD)	Source
ω_H	0.29 ± 0.09	Zhang et al., 2020
ω_M	0.23 ± 0.02	Present work
ω_{HM50}	0.21 ± 0.01	Present work
ω_{HM75}	0.23 ± 0.01	Present work
ω_{HM104}	0.17 ± 0.01	Present work
$m_{cell,H}^{dry}$ (10^{-11} g/cell)	2.14	Zhang et al., 2020
$m_{cell,M}^{dry}$ (10^{-11} g/cell)	1.43 ± 0.09	Present work
$m_{cell,HM50}^{dry}$ (10^{-11} g/cell)	2.08 ± 0.05	Present work
$m_{cell,HM75}^{dry}$ (10^{-11} g/cell)	2.27 ± 0.03	Present work
$m_{cell,HM104}^{dry}$ (10^{-11} g/cell)	2.46 ± 0.09	Present work
D_H (μm^3)	3.65 ± 0.01	Zhang et al., 2020
D_M (μm)	3.14 ± 0.02	Present work
D_{HM50} (μm)	3.43 ± 0.04	Present work
D_{HM75} (μm)	3.52 ± 0.15	Present work
D_{HM104} (μm)	3.40 ± 0.03	Present work

Note: Subscripts of H, HM, and M represent the heterotrophic, hetero-mixotrophic, and mixotrophic cultivations, respectively. The numbers 50, 75, and 104 indicate the light intensity in the light stage of hetero-mixotrophic cultivation.

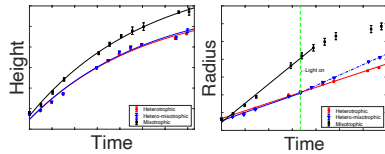
Table 3.

Source	O ₂ yield, Y_{O_2}		CO ₂ yield, Y_{CO_2}	
	Dark stage	Light stage	Dark stage	Light stage
	g O ₂ /g cell	g O ₂ /g cell	g CO ₂ /g cell	g CO ₂ /g cell
Heterotrophic	-0.64 ± 0.03		0.78 ± 0.03	
Mixotrophic				
$60 \mu\text{mol} \cdot \text{m}^{-2} \cdot \text{s}^{-1}$	0.04 ± 0.006		0.32 ± 0.05	
Hetero-mixotrophic				
$60 \mu\text{mol} \cdot \text{m}^{-2} \cdot \text{s}^{-1}$	-0.50 ± 0.02	-0.29 ± 0.02	0.49 ± 0.02	0.27 ± 0.02
$50 \mu\text{mol} \cdot \text{m}^{-2} \cdot \text{s}^{-1}$	-0.49 ± 0.02	-0.34 ± 0.02	0.52 ± 0.02	0.31 ± 0.01
$75 \mu\text{mol} \cdot \text{m}^{-2} \cdot \text{s}^{-1}$	-0.45 ± 0.02	-0.04 ± 0.006	0.43 ± 0.02	0.04 ± 0.005
$104 \mu\text{mol} \cdot \text{m}^{-2} \cdot \text{s}^{-1}$	-0.72 ± 0.04	0.001 ± 0.005	0.44 ± 0.02	-0.04 ± 0.005

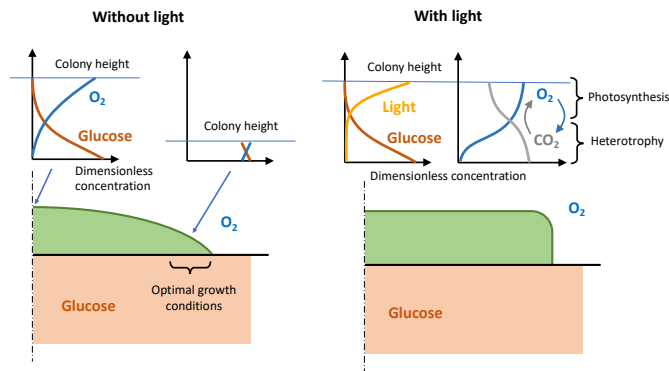
In-house device for immobilized culture with gas measurement



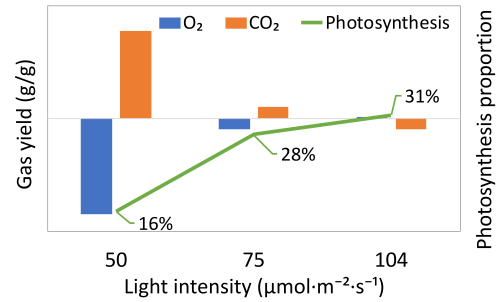
Colony development



Metabolic profile



Gas yield
(mass of gas per mass of biomass)



Photosynthesis proportion